THE JOURNAL OF PHYSICAL CHEMISTRY B

Article

pubs.acs.org/JPCB

Pulse Electron Double Resonance Detected Multinuclear NMR Spectra of Distant and Low Sensitivity Nuclei and Its Application to the Structure of Mn(II) Centers in Organisms

Eduardo M. Bruch,[†] Melissa T. Warner,[†,‡] Sébastien Thomine,[§] Leandro C. Tabares,[†] and Sun Un*[,†]

[†]Service de Bioénergétique, Biologie Structurale et Mécanismes (CNRS UMR-8221), Institut de Biologie et de Technologies de Saclay, CEA-Saclay, F-91191 Gif-sur-Yvette, France

[‡]Department of Biology, Tufts University, Medford, Massachusetts 02155, United States

[§]Institute for Integrative Biology of the Cell (I2BC), Saclay Plant Sciences, Université Paris-Saclay, CEA, CNRS, Université Paris-Sud, Gif-sur-Yvette, F-91198 France

Supporting Information

ABSTRACT: The ability to characterize the structure of metal centers beyond their primary ligands is important to understanding their chemistry. High-magnetic-field pulsed electron double resonance detected NMR (ELDOR-NMR) is shown to be a very sensitive approach to measuring the multinuclear NMR spectra of the nuclei surrounding Mn(II) ions. Resolved spectra of intact organisms with resonances arising from ^{55}Mn, ^{31}P, ^{1}H, ^{39}K, ^{35}Cl, ^{23}Na, and ^{14}N nuclei surrounding Mn^{2+} centers were obtained. Naturally abundant cellular ^{13}C could be routinely measured as well. The amplitudes of the ^{14}N and ^{2}H ELDOR-NMR spectra were found to be linearly dependent on the number of nuclei in the ligand sphere. The evolution of the Mn(II) ELDOR-NMR spectra as a function of excitation time was found to be best described by a saturation phenomenon rather than a coherently driven process. Mn(II) ELDOR-NMR revealed details about not only the immediate ligands to the Mn(II) ions but also more distant nuclei, providing a view of their extended structures. This will be important for understanding the speciation and chemistry of the manganese complexes as well as other metals found in organisms.

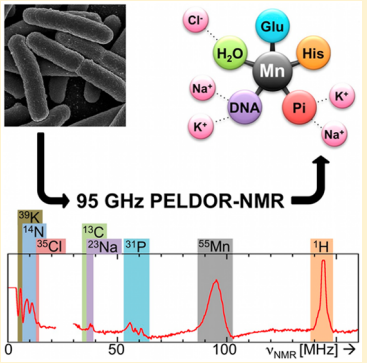

INTRODUCTION

The chemistry of transition metals is strongly affected by their ligands and environment. There are only a limited number of ways to probe the structures of such metal centers in complex disordered environments, such as those found in organisms. Recently, there has been much interest in how cellular inorganic Mn^{2+} complexes help certain bacteria resist radiation and oxidative stress.[1−5] Electron paramagnetic resonance (EPR) techniques have proven to be useful in this regard. High magnetic field continuous wave EPR (HFEPR) is a sensitive probe of the cellular Mn^{2+} itself.[3] ^{1}H and ^{31}P electron−nuclear double resonance (ENDOR)[2−4] and ^{14}N electron spin echo envelope modulation (ESEEM)[4] have been used to identify some of the prominent cellular Mn^{2+} ligands. These techniques have well-understood limitations.[6,7] For example, ENDOR techniques are technically ill-suited for detecting nuclei with small gyromagnetic ratios and are insensitive or blind to certain hyperfine couplings.[6] We will show that high magnetic field pulse electron double resonance detected NMR (ELDOR-NMR)[8] has certain advantages that will complement these other techniques. It has been used to study diverse systems to detect a wide variety of nuclei such as ^{14}N,[9−14] ^{17}O,[15−18] ^{61}Ni,[19] ^{55}Mn,[20] ^{51}V,[21] and ^{35,37}Cl.[22] It is possible to obtain broadband and resolved *in situ* NMR spectra of a wide variety of nuclei that surround cellular Mn^{2+} with very high sensitivity, even those with low natural isotopic abundance and low cellular concentrations. These include not only direct ligating nuclei but also distant ones. The spectra provide details about the extended structures and environments of these Mn^{2+} centers and, consequently, their potential chemistry and function.

ELDOR-NMR is a "pump-probe" based method. A microwave pump pulse excites a formally forbidden transition at frequency ν_{ex} that simultaneously "flips" both an electron and a nuclear spin to which it is magnetically coupled (Figure 1). This in turn modulates the amplitude of the EPR signal corresponding to electron-only spin transition, typically detected as a spin echo. The NMR spectrum of the nuclear spin is obtained by sweeping ν_{ex} while monitoring echo amplitude at a fixed frequency ν_{obs}. The measurements on the Mn(II, $S = 5/2$) ions described below were exclusively carried out on their $m_s = -1/2 \leftrightarrow +1/2$ transitions. This meant that expressions for the ELDOR-NMR of $S = 1/2$ centers previously derived by Schosseler and co-workers[8] and Florent and co-

Special Issue: Wolfgang Lubitz Festschrift

Received: February 17, 2015
Revised: March 2, 2015

DOI: 10.1021/acs.jpcb.5b01624
J. Phys. Chem. B XXXX, XXX, XXX−XXX

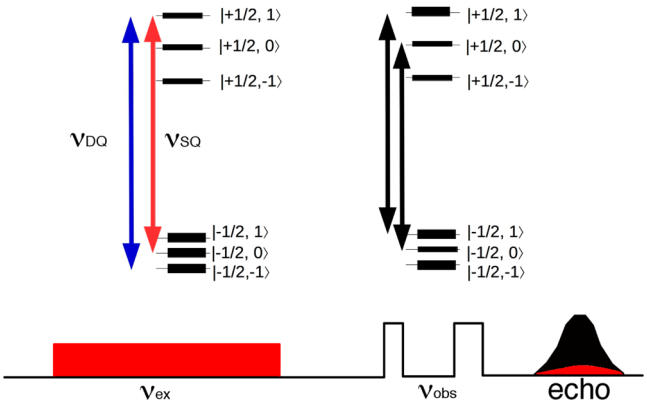

Figure 1. ELDOR-NMR experiment. A pulse with frequency ν_{ex} excites a forbidden transition (corresponding to either the red or blue arrows) inverting the populations of the two states. The thicknesses of the horizontal bars of the energy diagram represent relative populations before (left) and after (right) the pulse. The excitation of the forbidden transition reduces the intensity of the spin echo (from black to red). The energies corresponding to ν_{SQ} and ν_{DQ} are described in the text.

workers[10] could be used without modification. For a Mn(II) center coupled to a spin-1 nucleus, such as a ^{14}N atom, there are 12, not necessarily resolvable, ELDOR-NMR resonances. Their frequencies relative to the detection frequency (ν_{obs}) are[10]

$$\nu_{SQ} = \nu_{ex} - \nu_{obs} = \pm\nu_n \pm \frac{1}{2}A_n \pm \frac{3}{2}P_n \qquad (1)$$

$$\nu_{DQ} = \nu_{ex} - \nu_{obs} = \pm 2\nu_n \pm A_n$$

where A_n and P_n ($e^2q_{zz}Q/2I(2I-1)$) are the hyperfine and nuclear quadrupolar coupling constants of the nuclear spin with an NMR frequency, ν_n, and ν_{SQ} and ν_{DQ} correspond to single and double quantum nuclear spin transitions. Experimentally, using these two transitions, the hyperfine and quadrupolar couplings can be determined. All ELDOR-NMR spectra also share a large resonance at $\nu_{ex} = \nu_{obs}$ due to the excitation of the allowed transition by the pump pulse.

The maximum ELDOR-NMR effect occurs when ν_{ex} inverts the populations of the two states, that is, when the rotation angle, $\omega_f t$, of the ν_{ex} pulse is π, where

$$\omega_f = \omega_1 t\sqrt{I_f} \qquad (2)$$

and ω_1 is $g_e\beta_e B_1$, B_1 is the magnetic field generated by the microwave pulse, and I_f is the probability of the forbidden transition which is approximately

$$I_f \approx \frac{A_{n,zx}{}^2 + A_{n,zy}{}^2}{16\nu_n{}^2} \qquad (3)$$

where $A_{n,zx}$, $A_{n,zy}$, and $A_{n,zz}$ are the three components of the hyperfine tensor. To first order in the magnetic field, I_f is unaffected by the Mn(II) zero-field interaction.[23] There are a number of special cases. I_f is zero for purely isotropic hyperfine interactions, since $A_{n,zx}$ and $A_{n,zy}$ are zero. This is because such interactions do not mix nuclear spin states. In the case of an anisotropic dipolar hyperfine interaction, I_f will depend on the orientation of the dipolar axis relative to B_0 vanishing along both the parallel and perpendicular directions. Hence, the ELDOR-NMR line shape will deviate from the ideal Pake pattern with edges that are less sharp, yielding spectra that appear to be less resolved than ENDOR spectra.[24] For distant nonligand nuclei, their hyperfine couplings will be largely dipolar in character and their I_f will have a strong r^{-6} dependence. Hence, the detection of nuclei beyond the primary ligand sphere may be limited. For example, the directly bound water protons in $[Mn(H_2O)_6]^{2+}$ are approximately 3.1 Å from the metal center while the nearest solvent protons are about 5.3 Å and their I_f values will differ by a factor of 25 due to their difference in hyperfine couplings. This should lead to a strong suppression of the signal from the latter matrix protons reminiscent of similar suppression effects observed with the Davies ENDOR technique.

An interesting consequence of eq 3 is that isotopes of the same nuclei will have the same I_f, since both the hyperfine and Zeeman interaction have the same dependence on nuclear magnetogyric ratio, γ_n. This means that for a constant ω_1 the detection of the isotopes of the same atom, for example, protons and deuterons, will be equally sensitive. This also holds true for different nuclei that have the same dipolar coupling strength, since eq 3 does not depend on γ_n. By contrast, the efficiency of ENDOR experiments, which directly excite allowed NMR transitions (for example, between state $|+1/2, 0\rangle$ and $|+1/2, 1\rangle$ in Figure 1), depends directly on γ_n. Nuclei with smaller magnetogyric ratios require either more radio frequency power or longer pulse times. The former may pose technical problems including heating, while the latter may be limited by relaxation. For ELDOR-NMR measurements, which typically use frequency-tuned resonators, the pumping of the forbidden transitions involving low γ_n nuclei tend to be more efficient, since the difference ν_{ex} and ν_{obs} are smaller.

The intensity of a ELDOR-NMR resonance is given by[8]

$$h = 1 - \cos(\omega_1 t\sqrt{I_f}) \qquad (4)$$

Equation 4 is periodic with the oscillation frequency depending on I_f. To obtain maximum intensities, nuclei with different hyperfine couplings require different pump-pulse lengths. Long "high turn angle"[9] pump pulses can compensate for weak couplings but potentially at the cost of stronger ones. This in principle could lead to complex behavior that would make spectra difficult to analyze, let alone quantitate. As has been pointed out previously, when pulse times are long compared to relaxation effects, the excitation of the forbidden transitions is better described as a saturation phenomenon rather than a coherent polarization inversion (as implied by eq 4).[15] The temporal behavior in this case can be calculated using classical Bloch equations.[25] Such effects are likely to be important particularly for metal ions that have short transverse times, T_2.

In the following, we describe measurements that examine the application of ELDOR-NMR to organisms and related model complexes to understand the extended structure of cellular Mn(II) species. The same approach can be used to study other heterogeneous complex systems. We will address issues relating to (1) the sensitivity under practical experimental conditions, in particular, to low sensitivity and distant nuclei; (2) temporal behavior of the ELDOR-NMR resonances; and (3) spin quantitation.

MATERIALS AND METHODS

Cell Samples. The cells were grown in Erlenmeyer flasks with media occupying 20% of the total flask volume and agitated at 180 rpm. The optical density (OD) was followed

DOI: 10.1021/acs.jpcb.5b01624
J. Phys. Chem. B XXXX, XXX, XXX−XXX

spectrophotometrically at 600 nm using a UVIKON XL UV/vis double-beam spectrophotometer. *E. coli* DH5α was grown in TGY 2× medium at 37 °C until reaching a stationary phase. *D. radiodurans* cells were grown in TGY 2× medium at 32 °C. After achieving the desired OD, the cells were centrifuged for 5 min at 3000×*g* and the resulting pellets were washed three times with buffer (50 mM Tris, pH 8, 150 mM NaCl). The suspensions were then transferred into capillary quartz tubes (Bruker, bottom-beaded 95 GHz sample tube) and compacted by centrifugation; the amount of cells in the tube was enough to fill the microwave cavity (for more details, see ref 3). After frozen in liquid nitrogen, the samples were stored at 200 K until used. The samples were cooled in liquid nitrogen before they were loaded. This ensured that they were well frozen at all times. The viability of *E. coli* and *D. radiodurans* cells after being flash frozen in liquid nitrogen has been shown to be higher than 80%.[3,26]

Dry seeds from wild type *A. thaliana* were harvested from plants grown in potting soil (Tonerde PAM Argile, Brill, France) in a growth chamber at 21 °C with 60% humidity, under 180 μmol photon/(m^2 s) with a 16 h photoperiod and regular watering (2−3 times per week). After harvest, seeds were stored at 8 °C in a well-aerated dark room.

The Mn:DNA complex was prepared from salmon testes DNA (Sigma-Aldrich) dissolved in water (1−3 mg/mL) with a Mn^{2+} concentration of 50−150 μM.

Model Complexes. In the following, all solutions contained Mn(II) from $Mn(ClO_4)_2{\cdot}6H_2O$ (Sigma-Aldrich) and were pH adjusted using HCl and KOH. All solutions contained 50 μM Mn(II). $[Mn(H_2O)_6]^{2+}$ refers to a simple Mn(II) solution of 20% v/v glycerol and water. $[Mn(imidazole)_4]^{2+}$ was formed by mixing 1 M imidazole with 50 μM Mn(II) in 20% v/v glycerol and water and $[Mn(imidazole)_2(H_2O)_4]^{2+}$ with 50 mM imidazole.[12] $[Mn(glutamate)(H_2O)_4]^{1+}$ was formed in a solution of 50 μM Mn(II) and 100 mM potassium glutamate pH adjusted to 7.5. The 285 GHz EPR measurements showed no $[Mn(H_2O)_6]^{2+}$ present, and 95 GHz proton ENDOR measurement identified a complex having 3.6 water ligands. ELDOR-NMR measurements confirmed a single nitrogen ligand. This was consistent with the stoichiometry reported in the literature.[27]

EPR Spectroscopy. The 95 GHz ELDOR-NMR and ENDOR spectra were obtained at 6 K using a Bruker Elexsys II 680 EPR spectrometer equipped with a Bruker "Power upgrade 2", 500 W Amplifier Research radiofrequency amplifier and an Oxford Instruments CF935 flow cryostat. The ELDOR spectra were obtained by sweeping the frequency (ν_{ex}) of a 90 μs "high-turn-angle" pulse followed by standard spin−echo detection at ν_{obs} using either 120 and 240 or 300 and 600 ns pulses depending on the experiments. All ELDOR and ENDOR measurements were carried out using the highest magnetic-field Mn(II) hyperfine line, corresponding to the $m_S = -1/2$ $m_I = +5/2 \leftrightarrow m_S = +1/2$ $m_I = +5/2$ transition.

For broad ELDOR-NMR scans, the microwave cavity was tuned to the middle of the scan and modestly overcoupled to increase bandwidth. The length of the pump pulse was 50−90 μs with an intensity, ω_{1ex}, that varied from 0.3 to 3 × 10^6 rad s^{-1}, and the signal was detected using spin−echo detection using 120 and 240 ns pulses. For resolved ^{14}N spectra, ω_{1ex} was 0.5 × 10^6 rad s^{-1}. For ^{13}C, ^{2}H, ^{31}P, and ^{1}H, ω_1 was 3 × 10^7 rad s^{-1} and 300 and 600 ns pulses were used to detect the spin echo to achieve good resolution. Unless otherwise stated, quadratic or Gaussian baselines were subtracted from all of the ELDOR-NMR spectra.

Davies ENDOR[28] measurements were composed of a 200 ns microwave preparation and 20 μs radiofrequency pulses followed by a two-pulse echo detection (10 and 20 ns microwave pulses separated by 600 ns). Phase cycled three-pulse Mims ENDOR[29] measurements were comprised of two 20 ns microwave pulses separated by 300 ns followed by a 20 μs radiofrequency pulse and a final 20 ns microwave pulse.

Numerical solutions to the Bloch equations were based on the approach by Torrey.[30] There have been a number of other derivations of the solutions to these equations. We have found that some were more prone to numerical instabilities associated with digital accuracy and machine round-off errors. The procedure implemented by Mulkern and Williams[31] avoided such problems.

Density functional calculations were carried using program packages Gaussian 09 (revision B.01)[32] and ORCA (version 3.0.2).[33] The former was used to optimize geometries using the B3LYP/6-31+G(D,P) hybrid density functional and basis set and later to obtain the hyperfine coupling values using the PBE0/6-31+G(D,P) combination. All calculations included water solvation.

RESULTS AND DISCUSSION

Figure 2 shows the broadband 95 GHz 3T Mn(II) ELDOR-NMR spectra of Mn(II) centers in intact *E. coli* and *D. radiodurans* cells as well as *A. thaliana* seeds exhibiting a number of different resonances. These organisms typically have internal cytosolic concentrations of 50−200 μM, but the overall Mn^{2+} concentrations of the samples were only on the order of 10 μM. The difference reflected the packing efficiency of samples. However, only a few hours of acquisition were required to obtain all of the relevant features. Aside from ^{55}Mn, ^{31}P, and ^{1}H, which have been detected previously by ENDOR,[2−4] the ELDOR-NMR spectra had resonances arising from ^{39}K, ^{35}Cl, ^{23}Na, ^{14}N, and ^{13}C. With the exception of the ^{55}Mn resonances, the others were well separated and centered at their respective NMR frequencies, making their identification

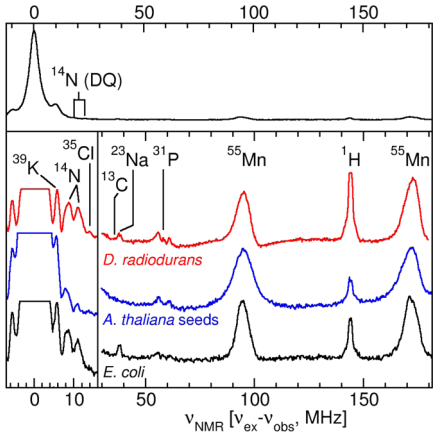

Figure 2. 95 GHz ELDOR-NMR spectra of *E. coli*, *D. radiodurans*, and *A. thaliana* seeds: (top) the complete *E. coli* spectrum from −10 to 180 MHz; (bottom right) the ×20 vertical expansions from 30 to 180 MHz and (bottom left) the −7 to 10 MHz regions of the spectra taken with low powers to better resolve the various components.

DOI: 10.1021/acs.jpcb.5b01624
J. Phys. Chem. B XXXX, XXX, XXX−XXX

trivial. ^{55}Mn was the only case where A_n was larger than ν_n, but its resonances could be assigned on other EPR measurements.

^{1}H and ^{31}P ELDOR-NMR organism resonances had resolved line shapes. Not unexpectedly, the ^{1}H spectra closely resembled the spectrum of $[Mn(H_2O)_6]^{2+}$ (Figure 3).[24] The pronounced

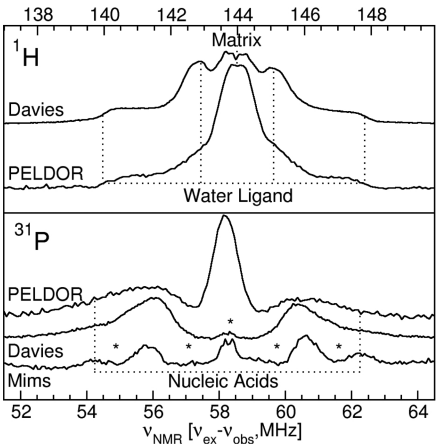

Figure 3. Comparison of the ^{1}H (top) and ^{31}P (bottom) regions of the ENDOR and ELDOR-NMR spectra of *D. radiodurans*. The asterisks mark the "blind spots" in the ENDOR spectra. The spectra have been arbitrarily vertically scaled.

matrix peak suggested that, contrary to expectations, ELDOR-NMR unlike Davies ENDOR was sensitive to protons with weak hyperfine couplings, such as those beyond the primary ligand sphere. This was also true for the ^{31}P phosphate signal. The resolved ^{31}P doublet ENDOR spectra of the organisms arose from directly bound phosphates. In the case of *D. radiodurans* (Figure 3), the shape of the resonances reflected contributions from nucleic acid phosphates (24%), fructose-1,6-bisphosphate (52%), and other phosphates, such as ortho- and polyphosphates (20%).[3] Consistent with theoretical expectations (see above), the ^{1}H and ^{31}P ELDOR-NMR spectra appeared less resolved at the edges than the Davies and Mims ENDOR spectra. For example, the shoulders of ^{31}P ELDOR-NMR resonance arising from nucleic acids were less distinct. However, the size of its matrix resonance appeared to better reflect the number of nearby nonligating phosphates (see below). A significant signal was expected, since a large fraction of the phosphate ligands had both a ligating and also one or more close-by nonligating phosphate groups.[3] As expected, unlike the Mims ENDOR spectrum, the ELDOR-NMR spectrum was free of any obvious blind spots (Figure 3).

The organisms also exhibited strong ^{14}N (I = 1) resonances. The low-power resolved doublet spectra (Figure 4) were simpler to interpret and quantitate (see below) than the corresponding ESEEM spectra.[4] The line shape of the *A. thaliana* seeds closely resembled that of $[Mn(glutamate)(H_2O)_4]^{+}$, while those of the bacteria more resembled the $([Mn(imidazole)_2(H_2O)_4]^{2+}$ resonance. The corresponding doublet splittings were 2.7 and 2.5 MHz, respectively, indicating that in both cases the resonances arose from nitrogen directly bound to Mn^{2+}.[12] In the case of *D. radiodurans*, the ^{14}N double quantum ν_{DQ} resonances were also detected, a doublet centered at $2\nu_{NMR,^{14}N}$ with a splitting of 4.9 MHz similar to those of $[Mn(imidazole)_2(H_2O)_4]^{2+}$ and $[Mn(glutamate)(H_2O)_4]^{+}$ (Figure 4, inset). On the basis of eq 1 and these measured values, A^{14}_N for *D. radiodurans* was

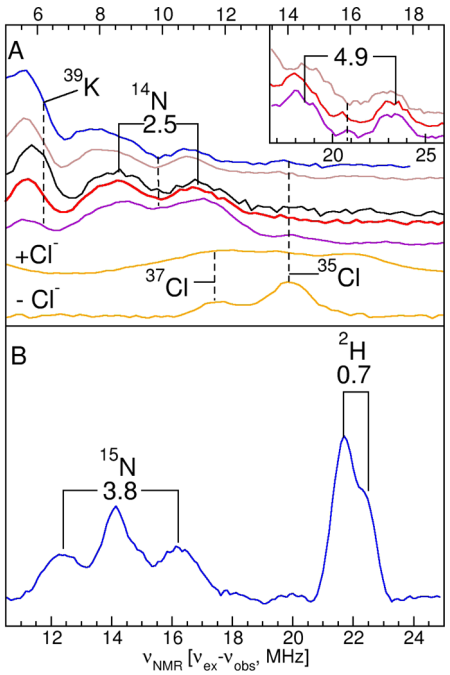

Figure 4. (A) Resolved ^{14}N ELDOR-NMR of *E. coli* (black), *D. radiodurans* (red), *A. thaliana* seeds (blue), $[Mn(imidazole)_2(H_2O)_4]^{2+}$ (violet), $[Mn(glutamate)(H_2O)_4]^{+}$ (brown), and 100 μM Mn(II) in 1 M perchloric acid (orange) with and without 100 mM chloride. The inset shows the corresponding ^{14}N ν_{DQ} transitions. (B) ^{15}N enriched *A. thaliana* seeds imbibed with 2% $^{2}H_2O$. The spectra have been arbitrarily scaled.

determined to be 2.5 MHz and P^{14}_N, less than 1 MHz. Measurements were also made on ^{15}N (I = 1/2) isotope enriched *Arabidopsis* seeds. Their spectra exhibited a well-resolved ν_{SQ} doublet with a separation of 3.8 MHz, corresponding to a coupling A^{14}_N of 2.7 MHz ($A^{14}_N = A^{15}_N\gamma^{14}_N/\gamma^{15}_N$), the same as the ^{14}N splitting implying that the P_{14N} were small for the seed nitrogens.

The prominent matrix peak in the *Arabidopsis* seed ^{15}N spectrum indicated that a significant fraction of the Mn^{2+} centers was inside nitrogen rich environments, namely, proteins or peptides. The appearance of the ^{15}N ELDOR-NMR spectrum was consistent with the observation that about 2/3 of all manganese containing proteins in the PDB database have at least one histidine ligand binding the metal. The doublet would correspond to directly bound histidine ring nitrogens and the matrix peak to the distal ring nitrogens. The latter would be about 4.3 Å from the metal ion and according to DFT calculation have an A^{15}_N of only a few kHz. Although there is insufficient information to identify the proteins or peptides involved, ^{15}N ELDOR-NMR is being used to probe the changes in the overall Mn^{2+} protein/peptide content during the hydration of dry seeds, the first step in germination. The uptake of water is being simultaneously monitored using $^{2}H_2O$ and ^{2}H ELDOR-NMR. The high sensitivity of this approach is shown in Figure 4B. Only 2% $^{2}H_2O$ in H_2O was needed to obtain readily detectable signals associated with isotope exchange at the level of the cellular Mn^{2+} inside the seeds.

Natural abundance ^{13}C (1%) nuclei could be routinely detected even in intact organisms and from the nonligating sucrose cryoprotectant used in $[Mn(H_2O)_6]^{2+}$ solution (Figure 5). The hyperfine couplings between ^{13}C nuclei and Mn(II) ions are likely to be small, but neither this nor the low

DOI: 10.1021/acs.jpcb.5b01624
J. Phys. Chem. B XXXX, XXX, XXX−XXX

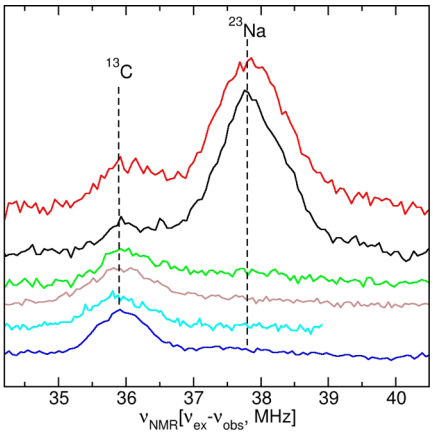

Figure 5. ^{13}C and ^{23}Na ELDOR-NMR spectra of *D. radiodurans* (red), *E. coli* (black), *Arabidopsis* seeds (green), $[Mn(glutamate)(H_2O)_4]^+$ (brown), $[Mn(imidazole)_4]^{2+}$ (cyan), and $[Mn(H_2O)_6]^{2+}$ in 500 mM sucrose (blue).

abundance of this isotope appeared to be a limiting factor to its detection. Natural abundance ^{13}C nuclei have been detected in ENDOR studies on purified proteins and solid-state materials (for examples, see refs 34 and 35). Previous ENDOR and ESEEM studies on organisms did report the detection of ^{13}C signals.[2−4] At lower observation frequencies (35 and 9 GHz), such as those used in some of these studies, it would have been difficult to resolve the ^{13}C resonance from the larger nearby one arising from ^{23}Na (100% natural abundance). The intensities of the organism ^{13}C spectra normalized to acquisition conditions were found to be comparable to those of 50 μM $[Mn(glutamate)(H_2O)_4]^+$ and $[Mn(imidazole)_4]^{2+}$. This suggested that a significant fraction of the Mn(II) ions in the organisms were bound to carbon containing environments, rather than to simple inorganic ligands. For *D. radiodurans* and *E. coli*, which both also had strong ^{14}N resonances, this again indicated that a significant number of Mn(II) ions are associated with carbon rich environments rather than simple inorganic ones, which corroborates our previous findings.[3,14]

In addition to ^{13}C, other distant nuclei were also detected in the organisms by ELDOR-NMR. The presence of resonances from Cl^-, K^+, and Na^+ (Figures 4 and 5) showed that the Mn(II) centers in the organisms were structured well beyond the primary ligand shell. The ^{35}Cl (13.7 MHz, 76% natural abundance) resonances were typically small and close to the more intense ones arising from ^{14}N. This also prevented the detection of the ^{37}Cl (11.4 MHz and 23% natural abundance) nuclei. Both isotopes have been detected by ELDOR-NMR on radicals having directly bound chloride atoms.[22] In order to confirm that ^{35}Cl could be detected at biologically relevant concentrations, 100 μM Mn(II) solutions containing 100 mM chloride were examined. No chloride resonances were detected in solutions having 500 mM sucrose or 20% glycerol. The organic cryoprotectants, which are used to obtain narrow well-defined Mn(II) EPR resonances, prevent direct chloride binding to the Mn(II) ions.[36] We have found that similar sharp spectra can also be obtained using 1 M perchloric acid instead. Ligand counting using Davies ENDOR confirmed that only $[Mn(H_2O)_6]^{2+}$ was present in such solutions. When 100 mM Cl^- was added to such solutions, strong, but very broad, unresolved resonances in the ^{37}Cl and ^{35}Cl NMR frequency region were detected (Figure 4A). They were more intense and broader than the corresponding ones found in the spectra of Mn(II) imidazole solutions and organisms. Mn(II) perchloric acid solutions with no chloride exhibited two weak, but sharp, resonances at the two chloride NMR frequencies with relative intensities roughly reflecting their isotopic abundance. The shape of the ^{35}Cl resonance matched those found in the Mn(II) imidazole solutions and organisms. DFT calculations were in close agreement. The calculated A^{35}_{Cl} for a directly bound chloride ion in $[Mn(H_2O)_5Cl]^+$ was [3.1, 3.2, 3.7] MHz with a P^{35}_{Cl} of −1 MHz. By contrast, the calculated A^{35}_{Cl} and P^{35}_{Cl} of a perchlorate anion hydrogen bound to $[Mn(H_2O)_6]^{2+}$ was [0.04, 0.05, 0.09] and −0.1 MHz, respectively. In such a case, the Mn(II)−Cl distance was 5.6 Å in the optimized geometry of this supercomplex. These measurements and calculations demonstrated that the detection of chloride ions associated with cellular Mn(II) was indeed reasonable.

^{39}K and ^{23}Na resonances were also present in the spectra of the organisms. Among the model complexes, they were only found when anionic ligands such as phosphate, carboxylates, and amino acids were present. This suggested that these cations were ionically bound to Mn(II) ligands, forming an extended structure. Although the intensities of ^{39}K resonances were

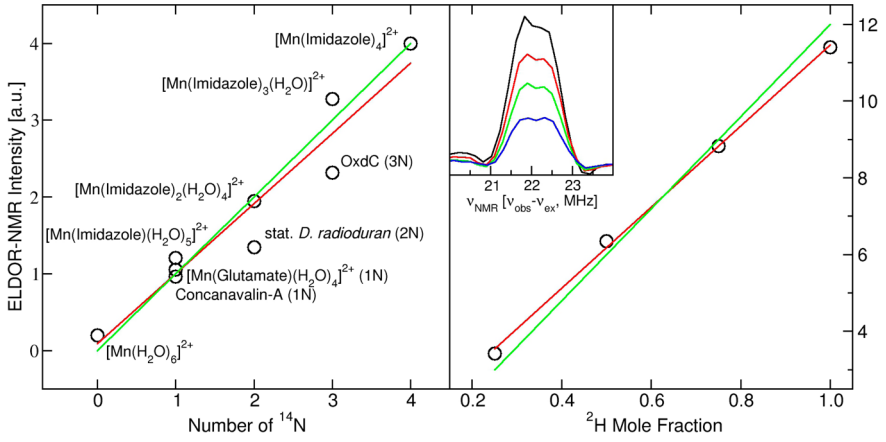

Figure 6. ^{14}N (left) and ^{2}H (right) ELDOR-NMR intensities as a function of the number of nuclei (circles). The ^{14}N data come from the indicated complexes and proteins and the ^{2}H from 50 μM Mn(II) and 250 mM sucrose in varying mixtures of $^2H_2O/^1H_2O$. The red lines are the regression fit of the data, and the green, the ideal correlations. The ^{2}H ELDOR-NMR spectra are shown in the inset. See refs 12 and 14 for detailed descriptions of the ^{14}N data.

DOI: 10.1021/acs.jpcb.5b01624
J. Phys. Chem. B XXXX, XXX, XXX−XXX

roughly equal among the organisms, ^{23}Na resonances varied (Figures 2, 4A, and 5). Their intensity ratios for *E. coli* and *Arabidopsis* seeds qualitatively followed the known sodium−potassium cellular concentration ratios of 1:40[37] and 1:170,[38] respectively.

These observations lead to the question of how quantitative such ELDOR-NMR measurements were in general. As we have noted before,[12,14] the intensity of ^{14}N ELDOR-NMR resonance was found to be proportional to the number of ^{14}N ligands. Figure 6 (left) summarizes the results from these and other previous measurements. Although there are some deviations, these results show that the number of nuclei can be determined to at least ±0.5 accuracy. At least in the case of the intact organisms, ELDOR-NMR provided a more direct manner to quantify nitrogen ligation than ESEEM.[4,14] A more controlled study was carried out on the quantification of ^{2}H by varying the $^2H_2O/^1H_2O$ mixture in solutions containing 50 μM Mn(II) and 200 mM sucrose. As Figure 6 (right) shows, the relationship between ELDOR-NMR amplitude and mole fraction of ^{2}H was highly linear. The linearity of the ELDOR-NMR response likely arises from the linear increase in the number of forbidden transitions associated with increasing number of coupled nuclei.

The intensities of the ELDOR-NMR resonances did not appear to strongly depend on the size of the hyperfine couplings nor did they exhibit periodic behavior as a function of the pump-pulse length as predicted by eq 4. A more thorough study was made using $[Mn(H_2O)_6]^{2+}$ and Mn:DNA complexes. The intensities of both the ^{1}H and ^{31}P ELDOR-NMR resonances rose quasi-exponentially nearly uniformly across the spectrum (Figures S1 and S2, Supporting Information). Limiting intensities were reached by 90 μs for ^{31}P and 50 μs for ^{1}H. Such a behavior suggested that the excitation of the forbidden transition was not being coherently driven but was being affected by spin relaxation. Since the transverse relaxation times, T_2, of the two Mn(II) complexes were 2 to 3 × 10^{-6} s and the $\omega_1 I_f^{1/2}$ were on the order of 10^4 to 10^5 rad s^{-1}, this seemed reasonable. The effect of relaxation on the excitation of the forbidden transitions was modeled by integrating Bloch equations using the method of Torrey.[30,31] This assumed that the forbidden transitions between the $m_s = \pm 1/2$ levels of a Mn(II) ion coupled to a $I = 1/2$ spin (^{31}P or ^{1}H) could be treated as selective excitations of a fictitious spin-1/2. The treatment of such a system is described by Schweiger and Jeschke.[39] As with previous calculations,[15] the relevant relaxation times were assumed to be the measured T_2 and T_1. The exact T_1 values were unimportant for the numerical calculations, since they were long, greater than 1 ms. The T_2 determined from two-pulse spin−echo measurements were between 2 and 3 μs for both model systems. The ω_1 values were determined from nutation measurements and the I_f calculated from hyperfine couplings obtained from simulations of the ENDOR data (see below and the Supporting Information) and equations given by Schossler and co-workers.[8] The only unknowns in the calculations were the inhomogeneous line shapes of the forbidden transitions. Good results were obtained by assuming a Gaussian shape. Only a single line width ($\Delta\omega_{fwhm,ex}$) of about 2.5 × 10^6 rad s^{-1} was needed to accommodate both the ^{31}P and ^{1}H measurements.

$[Mn(H_2O)_6]^{2+}$ and Mn:DNA presented two different cases. The ^{31}P hyperfine interactions of directly bound phosphate ligands are largely isotropic, while those of the water-ligand protons are essentially dipolar. As noted earlier, the isotropic component does contribute to the ELDOR-NMR response. In agreement with previous measurements,[24] the Davies ENDOR spectra of water-ligand protons were characterized by a hyperfine tensor with $A_\parallel = 7.9$ and $A_\perp = -2.7$ MHz (Figure S3, Supporting Information). There were also a number of smaller components arising from surrounding nonligating water protons. As Figure 7 shows by using these values and

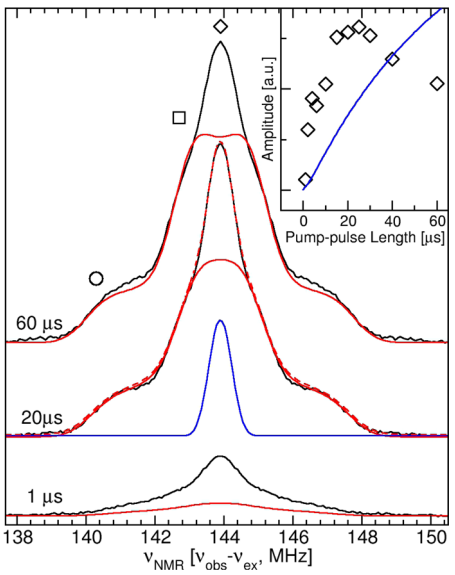

Figure 7. ^{1}H ELDOR-NMR spectra of $[Mn(H_2O)_6]^{2+}$ using 1, 20, and 60 μs pump pulses with a ω_1 value of 2.6 × 10^7 rad s^{-1} (black). The measured spectra have been symmetrized about ν_{n1H}. Their simulations based on the Bloch equations and $A_\parallel = 7.8$ and $A_\perp = -2.3$ MHz are shown in red. A common scaling factor has been applied to the simulations. Simulation of the matrix region at 20 μs using $A_\parallel = 1.4$ and $A_\perp = -0.7$ MHz is shown (blue), as well the sum of the two components (dash-red). The inset shows the evolution of the matrix region as a function of the pump-pulse length. The simulations assumed a $\Delta\omega_{fwhm,ex}$ value of 2.3 × 10^6, a T_2 value of 2.5 × 10^{-6} s, and a Gaussian inhomogeneous line width of 0.5 MHz for the matrix component and 1.0 MHz for the directly bound water protons.

incorporating relaxation effects, it was possible to calculate accurately the evolution of ELDOR-NMR spectra of the ligating water protons. A smaller $A_\perp$ value of −2.3 MHz yielded a better fit. This likely compensated for the influence of the other proton contributions (Figure S3, Supporting Information). Below 2 μs pulse lengths, the difference between calculation and experiment progressively became larger. A high level of agreement was also obtained for the ^{31}P Mn:DNA ELDOR-NMR spectra of the directly bound phosphate ligand. In this case, the Davies ^{31}P ENDOR spectra was composed of two components: one with $A_\parallel = 10.5$ and $A_\perp = 7.5$ MHz with a relative contribution of 44% and the other with $A_\parallel = 6.8$ and $A_\perp = 4.4$ MHz with a relative contribution of 55% (Figure S4, Supporting Information). Using these values and weights, we were able to reproduce exactly the pump-pulse length dependence of the ligating ^{31}P nuclei (Figure 8). In general, these calculations showed that the quasi-exponential non-periodic behavior was due to transverse relaxation times that were on the order of or shorter than ω_f^{-1}—that is the ELDOR-NMR of Mn(II) centers was characterized by a saturation phenomenon rather than a coherently driven process. This also moderated the sensitivity of the ELDOR-NMR intensities to the size of I_f and, hence, to the magnitude of the hyperfine couplings.

DOI: 10.1021/acs.jpcb.5b01624
J. Phys. Chem. B XXXX, XXX, XXX−XXX

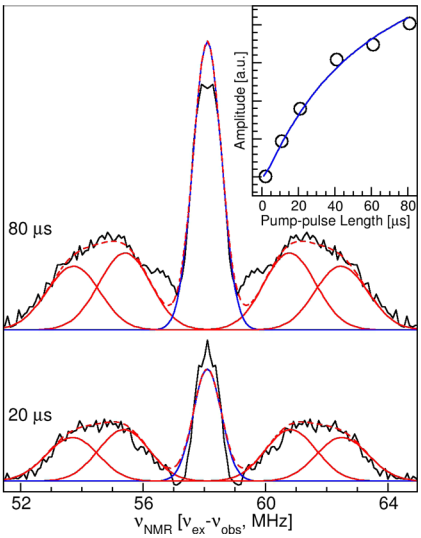

Figure 8. ^{31}P ELDOR-NMR spectra of the Mn(II):DNA complex using 80 and 10 μs pump pulses with a ω_1 value of 2.2 × 10^7 rad s^{-1}. The data have been symmetrized about ν_{n31P}. Simulation (solid red) is the sum of two contributions (dashed red) with (1) $A_{\|}$ = 10.5 and $A_{\perp}$ = 7.7 MHz and (2) $A_{\|}$ = 7.0 and $A_{\perp}$ = 4.4 MHz. The matrix region was simulated using $A_{\|}$ = 0.8 and $A_{\perp}$ = −0.4 MHz (blue). The inset shows the evolution of the matrix region as a function the pump-pulse length. The simulations assumed a $\Delta\omega_{fwhm,ex}$ value of 2.5 × 10^6 rad s^{-1} and a T_2 value of 1.5 × 10^{-6} s and a Gaussian inhomogeneous line width of 0.9 MHz for the matrix component and 1.5 MHz for the other two.

The matrix component of the Mn:DNA spectra could be isolated by taking the differences between the measurements and simulations. There are two interactions between the nonligand nucleic acid ^{31}P nuclei and the Mn(II) ions that are apparent from crystal structures (for examples, see refs 40 and 41). They involve the backbone phosphate groups neighboring the nucleotide nitrogen and phosphate metal binding sites, the closest being about 5 Å away. On average, each Mn(II) is directly bound by one nitrogen and 0.25 phosphates,[14] implying that there were at least one to two neighboring ^{31}P nuclei contributing to the matrix resonance. While this signal in the Davies and Mims ENDOR spectra was about 0.6−0.8 MHz wide (Figure S3, Supporting Information), the ELDOR-NMR resonance was somewhat broader, about 1.1 MHz. The coupling that best matched the pump-pulse length data was about 0.4 MHz (Figure 8, inset) consistent with a point-dipolar distance of 4.3 Å.

The matrix component of the $[Mn(H_2O)_6]^{2+}$ spectrum rose sharply, reaching a maximum at 20 μs and then falling (Figure 7, inset). Calculations have shown that there is a second shell of 18 water molecules between 4 and 5 Å from the metal center.[42] The corresponding proton hyperfine couplings from these secondary water protons would range from 0.5 to 1.0 MHz. The calculated pump-pulse length dependence for a dipolar hyperfine interaction of 0.7 MHz did not reproduce the data (Figure 7, inset). Hyperfine couplings consistent with the steepness of the initial rise would have exceeded the width of the matrix resonance itself; therefore, this did not seem likely. We were also unable to identify a set of reasonable parameters that allowed for the decrease in intensity. Although the isolated ^{1}H ELDOR-NMR matrix resonance could be simulated with a 0.7 MHz dipolar coupling, it was narrower than the corresponding Davies component (Figure 7 and Figure S3, Supporting Information). This suggested that evolution of the ELDOR-NMR matrix resonance might have been complicated by the multiple contributions.

From the simulation of the matrix resonances, it was possible to make a rough estimate of the number of matrix nuclei relative to those of the direct ligands. It is worth noting that the relatively low matrix intensities were largely a consequence of the smaller hyperfine coupling. From the 20 μs $[Mn(H_2O)_6]^{2+}$ spectrum, we estimated that the upper limit for the number of matrix protons detected was approximately 12 compared to the 48 predicted to be present from calculations.[42] The actual number under our experimental conditions was likely to be smaller than the calculated number. Cryoprotectant molecules have a strong effect on the EPR spectra of $[Mn(H_2O)_6]^{2+}$, indicating they are likely to be close to the metal centers and displace the secondary waters. Their proximity is supported by the observation of a ^{13}C resonance arising from them. For Mn:DNA, there was about one distant ^{31}P for every direct phosphate ligand or about 0.25 per Mn(II), smaller than one to two near neighbors anticipated from the crystal structures. Hence, for ^{1}H and ^{31}P, ELDOR-NMR appears to underestimate the number of matrix nuclei, at least using our relatively simple modeling. Further measurements on better-defined model systems and more detailed calculations are planned to gain a better understanding of this issue.

Although the ELDOR-NMR intensity of weakly coupled distant nuclei is not clearly understood, it is evident that nuclei well beyond 6 Å from the metal center can have robust ELDOR-NMR responses and can be readily detected. Minimally, this provides a comparative means for understanding the structure of Mn(II) binding sites, even within such complex environments as cells. For example, the ^{13}C resonance detected in all the organisms indicated that a significant number of Mn(II) ions exist in organic environments and the ^{15}N matrix resonance in ^{15}N enriched seeds could have only arisen from Mn(II) in protein or peptidic environments. Model data showed that the cationic resonances are only detected for metal centers that are bound by anionic ligands and their relatively ratios in the organism are consistent with their known concentrations. There are very few methods that are able to detect such secondary interactions of metal centers with cations and anions. Recently described 2D ELDOR-NMR measurements that correlate two nuclei would also greatly refine this approach.[15] Moreover, as Figure 6 demonstrates, under certain conditions, ELDOR-NMR can be used to count accurately the number of nuclei. This also suggests the possibility of using Mn(II) ELDOR-NMR as an indirect or surrogate probe of other cellular events, such as water intake in dormant desiccated seeds, as demonstrated in Figure 4B.

Mn^{2+} ELDOR-NMR is sensitive to a wide range of nuclei, even weakly interacting ones and those having low abundance. When coupled with high magnetic fields and microwave observation frequencies, only a few microliters of sample are required. The use of high magnetic fields also provides a high resolution which is especially important for resolving nuclei with low NMR frequencies. Although we have drawn examples from our study of Mn^{2+} speciation in cells, high-field ELDOR-NMR is well suited for other problems in biology and chemistry.[24] Previous work has shown that ELDOR-NMR also performs well with other metals.[17,24] It is likely to become a valuable approach to characterizing the extended structures of metal centers in complex environments.

DOI: 10.1021/acs.jpcb.5b01624
J. Phys. Chem. B XXXX, XXX, XXX−XXX

■ ASSOCIATED CONTENT

Supporting Information

^{1}H and ^{31}P ELDOR-NMR spectra as a function of pump-pulse length, ENDOR spectra, and simulations of $[Mn(H_2O)_6]^{2+}$ and Mn:DNA. This material is available free of charge via the Internet at http://pubs.acs.org.

■ AUTHOR INFORMATION

Corresponding Author

*E-mail: sun.un@cea.fr.

Notes

The authors declare no competing financial interest.

■ ACKNOWLEDGMENTS

This work was partially financed by the ANR (Contract No. 2011 BSV5-013-01 and 2011 BSV6-004-01), the French Infrastructure for Integrated Structural Biology (FRISBI, ANR-10-INSB-05-01), and the CNRS "Interface PCB" program. The spectrometer was funded by the Région Ile-de-France "Sesame" program, the CEA, and CNRS. We thank V. Ching and F. Leach for their input.

■ REFERENCES

(1) Barnese, K.; Gralla, E. B.; Valentine, J. S.; Cabelli, D. E. Biologically Relevant Mechanism for Catalytic Superoxide Removal by Simple Manganese Compounds. *Proc. Natl. Acad. Sci. U. S. A.* **2012**, *109*, 6892−6897.

(2) McNaughton, R. L.; Reddi, A. R.; Clement, M. H. S.; Sharma, A.; Barnese, K.; Rosenfeld, L.; Gralla, E. B.; Valentine, J. S.; Culotta, V. C.; Hoffman, B. M. Probing in Vivo Mn^{2+} Speciation and Oxidative Stress Resistance in Yeast Cells with Electron-Nuclear Double Resonance Spectroscopy. *Proc. Natl. Acad. Sci. U. S. A.* **2010**, *107*, 15335−15339.

(3) Tabares, L. C.; Un, S. *In Situ* Determination of Manganese(II) Speciation in *Deinococcus Radiodurans* by High Magnetic Field EPR: Detection of High Levels of Mn(II) Bound to Proteins. *J. Biol. Chem.* **2013**, *288*, 5050−5055.

(4) Sharma, A.; Gaidamakova, E. K.; Matrosova, V. Y.; Bennett, B.; Daly, M. J.; Hoffman, B. M. Responses of Mn^{2+} Speciation in *Deinococcus Radiodurans* and Escherichia Coli to γ-Radiation by Advanced Paramagnetic Resonance Methods. *Proc. Natl. Acad. Sci. U. S. A.* **2013**, *110*, 5945−5950.

(5) Culotta, V. C.; Daly, M. J. Manganese Complexes: Diverse Metabolic Routes to Oxidative Stress Resistance in Prokaryotes and Yeast. *Antioxid. Redox Signaling* **2013**, *19*, 933−944.

(6) Gemperle, C.; Schweiger, A. Pulsed Electron-Nuclear Double Resonance Methodology. *Chem. Rev.* **1991**, *91*, 1481−1505.

(7) Deligiannakis, Y.; Louloudi, M.; Hadjiliadis, N. Electron Spin Echo Envelope Modulation (ESEEM) Spectroscopy as a Tool to Investigate the Coordination Environment of Metal Centers. *Coord. Chem. Rev.* **2000**, *204*, 1−112.

(8) Schosseler, P.; Wacker, T.; Schweiger, A. Pulsed ELDOR Detected NMR. *Chem. Phys. Lett.* **1994**, *224*, 319−324.

(9) Potapov, A.; Epel, B.; Goldfarb, D. A Triple Resonance Hyperfine Sublevel Correlation Experiment for Assignment of Electron-Nuclear Double Resonance Lines. *J. Chem. Phys.* **2008**, *128*, 052320.

(10) Florent, M.; Kaminker, I.; Nagarajan, V.; Goldfarb, D. Determination of the ^{14}N Quadrupole Coupling Constant of Nitroxide Spin Probes by W-Band ELDOR-Detected NMR. *J. Magn. Reson.* **2011**, *210*, 192−199.

(11) Potapov, A.; Lancaster, K. M.; Richards, J. H.; Gray, H. B.; Goldfarb, D. Spin Delocalization over Type Zero Copper. *Inorg. Chem.* **2012**, *51*, 4066−4075.

(12) Un, S. Structure and Nature of Manganese(II) Imidazole Complexes in Frozen Aqueous Solutions. *Inorg. Chem.* **2013**, *52*, 3803−3813.

(13) Nagy, N. V.; Van Doorslaer, S.; Szabó-Plánka, T.; Van Rompaey, S.; Hamza, A.; Fülöp, F.; Tóth, G. K.; Rockenbauer, A. Copper(II)-Binding Ability of Stereoisomeric Cis- and Trans-2-Aminocyclohexanecarboxylic Acid-L-Phenylalanine Dipeptides. A Combined CW/pulsed EPR and DFT Study. *Inorg. Chem.* **2012**, *51*, 1386−1399.

(14) Bruch, E. M.; Thomine, S.; Tabares, L. C.; Un, S. Variations in Mn(II) Speciation among Organisms: What Makes D. Radiodurans Different. *Metallomics* **2015**, *7*, 136−144.

(15) Kaminker, I.; Wilson, T. D.; Savelieff, M. G.; Hovav, Y.; Zimmermann, H.; Lu, Y.; Goldfarb, D. Correlating Nuclear Frequencies by Two-Dimensional ELDOR-Detected NMR Spectroscopy. *J. Magn. Reson.* **2014**, *240*, 77−89.

(16) Rapatskiy, L.; Cox, N.; Savitsky, A.; Ames, W. M.; Sander, J.; Nowaczyk, M. M.; Rögner, M.; Boussac, A.; Neese, F.; Messinger, J.; et al. Detection of the Water-Binding Sites of the Oxygen-Evolving Complex of Photosystem II Using W-Band ^{17}O Electron-Electron Double Resonance-Detected NMR Spectroscopy. *J. Am. Chem. Soc.* **2012**, *134*, 16619−16634.

(17) Fittipaldi, M.; García-Rubio, I.; Trandafir, F.; Gromov, I.; Schweiger, A.; Bouwen, A.; Van Doorslaer, S. A Multi-Frequency Pulse EPR and ENDOR Approach to Study Strongly Coupled Nuclei in Frozen Solutions of High-Spin Ferric Heme Proteins. *J. Phys. Chem. B* **2008**, *112*, 3859−3870.

(18) Klein, E. L.; Raitsimring, A. M.; Astashkin, A. V.; Rajapakshe, A.; Johnson-Winters, K.; Arnold, A. R.; Potapov, A.; Goldfarb, D.; Enemark, J. H. Identity of the Exchangeable Sulfur-Containing Ligand at the Mo(V) Center of R160Q Human Sulfite Oxidase. *Inorg. Chem.* **2012**, *51*, 1408−1418.

(19) Flores, M.; Agrawal, A. G.; van Gastel, M.; Gärtner, W.; Lubitz, W. Electron-Electron Double Resonance-Detected NMR to Measure Metal Hyperfine Interactions: 61Ni in the Ni-B State of the [NiFe] Hydrogenase of Desulfovibrio Vulgaris Miyazaki F. *J. Am. Chem. Soc.* **2008**, *130*, 2402−2403.

(20) Kulik, L.; Epel, B.; Messinger, J.; Lubitz, W. Pulse EPR, 55Mn-ENDOR and ELDOR-Detected NMR of the S_2-State of the Oxygen Evolving Complex in Photosystem II. *Photosynth. Res.* **2005**, *84*, 347−353.

(21) Zamani, S.; Meynen, V.; Hanu, A.-M.; Mertens, M.; Popovici, E.; Van Doorslaer, S.; Cool, P. Direct Spectroscopic Detection of Framework-Incorporated Vanadium in Mesoporous Silica Materials. *Phys. Chem. Chem. Phys.* **2009**, *11*, 5823.

(22) Banerjee, D.; Paniagua, J. C.; Mugnaini, V.; Veciana, J.; Feintuch, A.; Pons, M.; Goldfarb, D. Correlation of the EPR Properties of Perchlorotriphenylmethyl Radicals and Their Efficiency as DNP Polarizers. *Phys. Chem. Chem. Phys.* **2011**, *13*, 18626−18637.

(23) Bir, G. L. Intensity of Allowed and Forbidden Electron Paramagnetic Lines. *Sov. Phys.-Solid State* **1964**, *5*, 1628−1635.

(24) Cox, N.; Lubitz, W.; Savitsky, A. W-Band ELDOR-Detected NMR (EDNMR) Spectroscopy as a Versatile Technique for the Characterisation of Transition Metal−ligand Interactions. *Mol. Phys.* **2013**, *111*, 2788−2808.

(25) Hovav, Y.; Feintuch, A.; Vega, S. Dynamic Nuclear Polarization Assisted Spin Diffusion for the Solid Effect Case. *J. Chem. Phys.* **2011**, *134*, 074509.

(26) Dumont, F.; Marechal, P.-A.; Gervais, P. Cell Size and Water Permeability as Determining Factors for Cell Viability after Freezing at Different Cooling Rates. *Appl. Environ. Microbiol.* **2004**, *70*, 268−272.

(27) Chung, L.; Rajan, K. S.; Merdinger, E.; Grecz, N. Coordinative Binding of Divalent Cations with Ligands Related to Bacterial Spores. *Biophys. J.* **1971**, *11*, 469−482.

(28) Davies, E. R. A New Pulse Endor Technique. *Phys. Lett. A* **1974**, *47*, 1−2.

(29) Mims, W. B. Pulsed Endor Experiments. *Proc. R. Soc. London, Ser. A* **1965**, *283*, 452−457.

(30) Torrey, H. C. Transient Nutations in Nuclear Magnetic Resonance. *Phys. Rev.* **1949**, *76*, 1059−1068.

(31) Mulkern, R. V.; Williams, M. L. The General Solution to the Bloch Equation with Constant RF and Relaxation Terms: Application to Saturation and Slice Selection. *Med. Phys. 20*, 5−13.

DOI: 10.1021/acs.jpcb.5b01624
J. Phys. Chem. B XXXX, XXX, XXX−XXX

(32) Frisch, M. J.; Trucks, G. W.; Schlegel, H. B.; Scuseria, G. E.; Robb, M. A.; Cheeseman, J. R.; Scalmani, G.; Barone, V.; Mennucci, B.; Petersson, G. A.; et al. *Gaussian 09*, revision B.01; Gaussian, Inc.: Wallingford, CT, 2010.
(33) Neese, F. The ORCA Program System. *Wiley Interdiscip. Rev.: Comput. Mol. Sci.* **2012**, *2*, 73−78.
(34) Houseman, A. L. P.; Oh, B. H.; Kennedy, M. C.; Fan, C.; Werst, M. M.; Beinert, H.; Markley, J. L.; Hoffman, B. M. Nitrogen-14,15, Carbon-13, Iron-57, and Proton-Deuterium Q-Band ENDOR Study of Iron-Sulfur Proteins with Clusters That Have Endogenous Sulfur Ligands. *Biochemistry* **1992**, *31*, 2073−2080.
(35) V. Duijn-Arnold, A.; Zondervan, R.; Schmidt, J.; Baranov, P. G.; Mokhov, E. N. Electronic Structure of the N Donor Center in 4H -SiC and 6H-SiC. *Phys. Rev. B* **2001**, *64*, 85206.
(36) Un, S.; Sedoud, A. High-Field EPR Study of the Effect of Chloride on Mn^{2+} Ions in Frozen Aqueous Solutions. *Appl. Magn. Reson.* **2009**, *37*, 247−256.
(37) Shabala, L.; Bowman, J.; Brown, J.; Ross, T.; McMeekin, T.; Shabala, S. Ion Transport and Osmotic Adjustment in Escherichia Coli in Response to Ionic and Non-Ionic Osmotica. *Environ. Microbiol.* **2009**, *11*, 137−148.
(38) Young, L. W.; Westcott, N. D.; Attenkofer, K.; Reaney, M. J. T. A High-Throughput Determination of Metal Concentrations in Whole Intact *Arabidopsis Thaliana* Seeds Using Synchrotron-Based X-Ray Fluorescence Spectroscopy. *J. Synchrotron Radiat.* **2006**, *13*, 304−313.
(39) Schweiger, A.; Jeschke, G. *Principles of Pulse Electron Paramagnetic Resonance*; Oxford University Press: New York, 2001.
(40) Millonig, H.; Pous, J.; Gouyette, C.; Subirana, J. A.; Campos, J. L. The Interaction of Manganese Ions with DNA. *J. Inorg. Biochem.* **2009**, *103*, 876−880.
(41) Vasudevan, D.; Chua, E. Y. D.; Davey, C. A. Crystal Structures of Nucleosome Core Particles Containing the "601" Strong Positioning Sequence. *J. Mol. Biol.* **2010**, *403*, 1−10.
(42) Yagüe, J. I.; Mohammed, A. M.; Loeffler, H.; Rode, B. M. Classical and Mixed Quantum Mechanical/Molecular Mechanical Simulation of Hydrated Manganous Ion. *J. Phys. Chem. A* **2001**, *105*, 7646−7650.

DOI: 10.1021/acs.jpcb.5b01624
J. Phys. Chem. B XXXX, XXX, XXX−XXX